RSC Advances

PAPER

View Article Online
View Journal | View Issue

Check for updates

Cite this: *RSC Adv.*, 2026, **16**, 30145

An injectable hyaluronic acid hydrogel integrating Fe(III)-coordination and polymyxin B grafts for accelerated healing of infected diabetic wounds

Mingchen Zhang,†[a] Wei Zhao,†[bc] Yang Zhou,[bc] Ruiting Shen,[a] Yiqiong Sun,[a] Lei Jiang*[bcd] and Jiantao Zhang *[cd]

Received 14th April 2026
Accepted 26th May 2026

DOI: 10.1039/d6ra03137d

rsc.li/rsc-advances

Diabetic wounds are a serious and increasingly prevalent complication in patients with diabetes, characterized by impaired skin regeneration. A major challenge for effective healing is recurrent bacterial infection, which often resists conventional treatment strategies. In this study, we grafted polymyxin B onto hyaluronic acid and employed Fe^{3+}–EDTA as a cross-linking agent to fabricate HA-B@Fe hydrogels *via* ionic interactions. Based on the reversible and dynamic coordination between Fe^{3+} ions and the carboxyl groups of the hyaluronic acid, the resulting hydrogels exhibited shear-thinning behavior and excellent injectability. Based on the combined effects of polymyxin B and Fe^{3+}, the HA-B@Fe hydrogel exhibited potent antimicrobial activity against a broad spectrum of bacteria, achieving >99% bactericidal rates against *Escherichia coli* (*E. coli*) and >94% against *Staphylococcus aureus* (*S. aureus*). In addition, the HA-B@Fe hydrogel demonstrated great biocompatibility, and showed significant therapeutic efficacy in a diabetic mouse wound model. The mice treated with HA-B@Fe showed a marked reduction in wound size (down to 19%), compared to a residual wound size of 32% in group treated with commercial dressings at day 7. Histopathological analysis further confirmed that HA-B@Fe treatment promoted epidermal regeneration and collagen fiber deposition, suggesting its potential as a promiseing strategy for the clinical treatment of diabetic wounds.

Open Access Article. Published on 03 June 2026. Downloaded on 6/9/2026 5:49:35 AM.
This article is licensed under a Creative Commons Attribution-NonCommercial 3.0 Unported Licence.

1 Introduction

Diabetic chronic wounds are a major complication of diabetes, characterized by a high incidence, delayed and impaired healing, and a high risk of recurrence.[1,2] Their poor healing outcomes are due to multiple pathological factors, including persistent hyperglycemia, exacerbated oxidative stress, chronic inflammation, and increased infection susceptibility. Collectively, these factors disrupt normal skin regeneration processes and hinder restoration of tissues through physiological repair mechanisms.[3] As a result, diabetic wounds become highly susceptible to recurrent bacterial infections, which further impede healing, trigger intensified inflammation, and ultimately perpetuate a vicious cycle of non-healing.[4,5] Therefore, effective control of bacterial infection is of great significance for the prevention and treatment of diabetic chronic wounds and form the foundation for the development of targeted wound dressings.

In clinical practice, bacterial infections are usually treated with antibiotics. However, the overuse and misuse of antibiotics have rapidly accelerated the emergence of bacterial resistance, which is now recognized as a major global health concern.[6,7] Antimicrobial resistance has escalated into a public health crisis, with projections indicating it could cause up to 10 million deaths annually by 2050, ranking it among the top three threats to human health.[8] Bacterial infections represent a significant and potentially severe complication, contributing to the growing burden on public health challenge and straining healthcare system worldwide. In the context of diabetic chronic wounds, bacterial infections are particularly problematic due to their recurrence and persistence, further complicating wound healing and patient outcomes. Therefore, there is an urgent need to develop advanced antimicrobial strategies to prevent microbial contamination of wounds. In recent years, antimicrobial peptides (AMPs) have attracted extensive attention owing to their broad-spectrum antimicrobial activity and low potential for inducing drug resistance.[9] The amine groups ($-NH_2$) in their molecular structure can be protonated, conferring them with cationic properties. These positive charges enable selective adsorption onto negatively charged bacteria surface

[a]*Department of Endocrinology and Metabolism, Ningbo No. 2 Hospital, Ningbo 315010, PR China*

[b]*Laboratory of Advanced Theranostic Materials and Technology, Ningbo Institute of Materials Technology and Engineering, Chinese Academy of Sciences, Ningbo 315201, PR China. E-mail: jianglei@nimte.ac.cn*

[c]*Ningbo Cixi Institute of Biomedical Engineering, Cixi 315300, PR China*

[d]*Zhejiang Key Laboratory of Biopharmaceutical Contact Materials, Ningbo 315201, China. E-mail: zhangjiantao@nimte.ac.cn*

† M. Z. and W. Z. contributed equally to this work.

© 2026 The Author(s). Published by the Royal Society of Chemistry

Open Access Article. Published on 03 June 2026. Downloaded on 6/9/2026 5:49:35 AM. This article is licensed under a Creative Commons Attribution-NonCommercial 3.0 Unported Licence.

through electrostatic interactions, ultimately disrupting the integrity and biological functions of the bacterial cell membrane.[10] The unique antibacterial mechanism of AMPs endows them several advantages, including broad-spectrum efficiency, rapid bactericidal action and a low susceptibility to induce drug resistance. Additionally, AMPs can enhance immune responses and accelerate wound healing. Therefore, AMPs represent a new class of antimicrobial agents with the potential to address the global challenge of antibiotic resistance. Their incorporation into wound dressings can offer an effective solution for the clinical management of chronic wound infections. For instance, AMPs have been loaded into hyaluronic acid/gelatin hydrogels to develop antibacterial hydrogel systems. Experimental study on infected mouse wound model have shown that AMPs-loaded hydrogels exhibit significant therapeutic effect.[11] In addition, functionalized nanocellulose membranes loaded with the AMP, PLNC8 αβ, have been used to treat wound infections. In a porcine wound infection model, these membranes demonstrated strong antibacterial activity, effectively eradicating the infection while simultaneously promoting wound reepithelialisation.[12] Although AMPs offer promising potential by effectively killing bacteria without inducing significant resistance, their clinical application requires delivery systems capable of maintaining sustained antibacterial activity.

Hydrogels have emerged as a particularly attractive platform, as their highly hydrated three-dimensional networks can not only serve as reservoirs for controlled AMP release but also provide a moist environment conducive to tissue repair. Consequently, hydrogels-based wound dressings with enhanced biological functions are commonly used to promote wound healing.[13,14] In current clinical practice, various natural polymers, such as silk,[15] collagen,[16] and hyaluronic acid[17] as well as synthetic polymers including poly(vinyl alcohol)[18] and polyvinylpyrrolidone [19] are considered as potential materials for tissue engineering applications. Natural polymeric materials have excellent biocompatibility and biodegradability, making them important candidates for wound therapy. Hyaluronic acid (HA), a major component of the extracellular matrix (ECM), has been widely used in biomedical engineering due to its involvement in biological process, including anti-inflammatory activity, wound healing and matrix organization.[20] Moreover, the abundance of carboxyl groups in the structure of HA provides opportunities for structural modification and offers numerous cross-linking sites. For instance, an injectable multifunctional hydrogel composed of dopamine-grafted HA and phenylboronic acid-grafted methylcellulose has been developed to promote diabetic wound repair.[21] *In vivo* experiments demonstrated that the HA-based hydrogel effectively reduced the expression of CD68 by promoting collagen deposition and granulation tissue regeneration. Despite these advances, the direct integration of potent AMPs into HA-based networks to achieve sustained, localized bacterial clearance remains an area warranting further exploration.

In this study, we developed a polymyxin B-grafted hyaluronic acid (HA-B) and an injectable HA-B@Fe hydrogel crosslinked *via* Fe^{3+}–EDTA coordination. The hydrogel formation is based on physical coordination between Fe^{3+} ions and carboxyl groups on HA, where reversible metal–carboxyl interactions impart shear-thinning behavior, enabling injectability. The incorporation of polymyxin B significantly enhanced the antibacterial activity. The Fe^{3+}–EDTA crosslinkers play dual roles: maintaining the integrity of the hydrogel and enabling sustained release of antibacterial Fe^{3+} complexes during biodegradation. This design endows the HA-B@Fe hydrogel with exceptional efficacy against *Staphylococcus aureus* (*S. aureus*) and *Escherichia coli* (*E. coli*). Furthermore, its interconnected porous structure facilitates nutrient and waste exchange between cells and surrounding tissues, while exhibiting excellent biocompatibility. The HA-B@Fe hydrogel demostrated therapeutic efficacy on diabetic wound in mice (Scheme 1). Overall, this work underscores the promising translational potential of AMP-functionalized HA hydrogels for the clinical management of chronic wounds and provides a novel paradigm for the design of bioactive HA-based materials for biomedical applications.

2 Experimental

2.1 Materials

Hyaluronic acid (HA, 200–400 kDa), dipotassium hydrogen phosphate, potassium phosphate, NaCl were obtained from Shanghai Maclin Biochemical Technology Co., Ltd, 1-(3-dimethylaminopropyl)-3-ethylcarbodiimide hydrochloride (EDC HCl) were purchased from Shanghai Aladdin Biochemical Technology Co., Ltd, Dulbecco's modified Eagle's medium (DMEM), fetal bovine serum (FBS), penicillin/streptomycin (PS), and trypsin solution were purchased from Gibco (USA). CCK-8 Kit, phosphate-buffered saline (PBS) solution, and Calcein-AM kit were purchased from Beyotime Biotechnology (China). SYTO 9/propidium iodide kit was purchased from Thermo Fisher Scientific (USA). Tryptic Soy Broth (TSB) and Tryptone Soy Agar (TSA) were purchased from Oxoid (UK). DI water (the conductivity is 1 μS cm^{-1}) was used for all experiments. The bacterial strains *S. aureus* (ATCC 6835) and *E. coli* (ATCC 25922) were obtained from Fenghui Biotechnology Co, Ltd (China). Mouse fibroblast cells (L929 cell) were obtained from Haixing Biosciences (China). ICR mice (male, 18–22 g, 4 weeks-old) were obtained from Beijing Vital River Laboratory Animal Technology Co., Ltd. The animal study protocol was approved by the Guoke Ningbo Life Science and Health Industry Research Institute (GK-2024-XM-1048 and 09-24-2024).

2.2 Synthesis and characterization of HA-B

The HA-B conjugate was synthesized by dissolving 0.5 g hyaluronic acid (HA) in 50 mL of 0.1 M MES buffer (pH 5.5), followed by the addition of 0.05 g EDC and 0.05 g HOBt under continuous stirring to activate the carboxyl groups. Separately, 0.1 g polymyxin B sulfate was dissolved in 5 mL MES buffer and then slowly added dropwise to the activated HA solution. The reaction was allowed to proceed at room temperature for 24 h with magnetic stirring. The reaction mixture was dialyzed (MWCO 8–14 kDa) against deionized water for 72 h and then freeze-dried for subsequent use. The chemical structure of HA-B

 © 2026 The Author(s). Published by the Royal Society of Chemistry

Open Access Article. Published on 03 June 2026. Downloaded on 6/9/2026 5:49:35 AM.
This article is licensed under a Creative Commons Attribution-NonCommercial 3.0 Unported Licence.

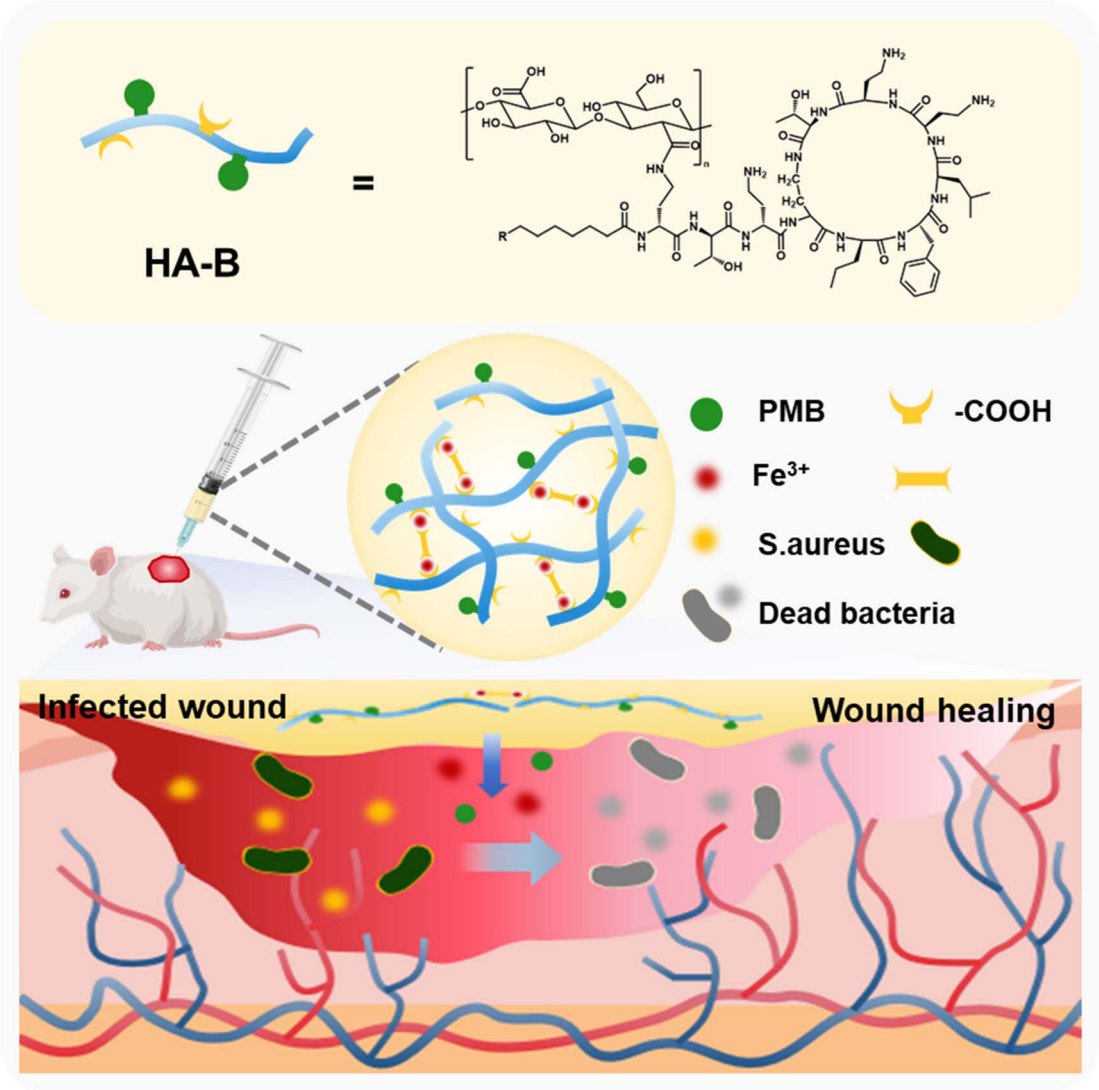

Scheme 1 Schematic illustration of the preparation of HA-B@Fe hydrogel and its proposed mechanism in promoting diabetic wound healing.

was confirmed by Fourier transform infrared (FTIR) spectroscopy (Agilent Cary 660, USA) and proton nuclear magnetic resonance (^{1}H NMR) spectroscopy (Bruker ADVANCE III, 400 MHz, Germany). FTIR spectra were recorded with 32 scans at a resolution of 4 cm^{-1} over the wavenumber range of 4000–400 cm^{-1}. For ^{1}H NMR spectroscopy, D_2O was used as the deuterated solvent, and spectra were acquired with 64 scans at a resonance frequency of 400 MHz.

2.3 Fabrication and characterization of the hydrogel

The HA-B@Fe hydrogel was fabricated using the following procedure: HA-B was suspended in deionized (DI) water at concentrations of 1, 2, and 3% (w/v) at room temperature to form dilute solutions. Next, $Fe_2(SO_4)_3$ and EDTA were dissolved in DI water to prepare a Fe^{3+}–EDTA complex solution, with both Fe^{3+} and EDTA at a molar concentration of 0.05 mol L^{-1}. Finally, 2 mL of the HA-B solution was mixed with 400 μL of Fe^{3+}–EDTA complex solution under magnetic stirring to obtain a homogeneous HA-B@Fe hydrogel. The resulting hydrogels were designated as HA-B_1@Fe, HA-B_2@Fe, and HA-B_3@Fe according to the concentration of HA-B. The gelling time of the hydrogel was assessed by the vial inversion method. The pregel solution was considered gelled when it no longer flowed upon inversion of the vial. The internal microstructure of the hydrogels was examined by scanning electron microscopy (SEM) using a Regulus 8230 instrument (Hitachi, Japan). Prior imaging, the samples were freeze-dried, mounted on conductive adhesive tape, and sputter-coated with a thin layer of gold to enhance the conductivity.

2.4 Mechanical and self-healing properties of hydrogels

The rheological properties of HA-B_1@Fe, HA-B_2@Fe, and HA-B_3@Fe hydrogels were assessed using a rheometer (TA, DHR-2, USA) equipped with a 20 mm parallel plate geometry. The tests conducted included a time sweep (120 s at 1% strain, 10 rad s^{-1} frequency), strain sweep (1–1500% strain at 10 rad s^{-1}

Open Access Article. Published on 03 June 2026. Downloaded on 6/9/2026 5:49:35 AM. This article is licensed under a Creative Commons Attribution-NonCommercial 3.0 Unported Licence.

frequency), alternate time-sweep (3.5 cycles of alternating 1% and 3000% strain, with each cycle lasting 30 s at 10 rad s^{-1} frequency), and flow sweep (0.1% stain at a range of angular frequencies). All experiments were performed at 25 °C, with a 500 μm gap and 300 μL of hydrogel per test.

2.5 Cell viability assay

The cytotoxicity and viability of L929 fibroblast cells were evaluated using hydrogel extracts through a Cell Counting Kit-8 (CCK-8) assay and Calcein-AM fluorescent staining. For the CCK-8 assay, cells were cultured in 10% hydrogel extract for 24, 48, and 72 hours. After each incubation period, CCK-8 reagent was added according to the manufacturer's protocol. Following 1 h of incubation in a cell culture incubator, absorbance was measured at 450 nm using a microplate reader. Cell viability was then calculated based on the absorbance values using the following equation:

$$\text{Cell viability rate}(\%) = \frac{(A_t - A_0)}{(A_{c1} - A_0)} \times 100\%$$

A_t, A_0 and A_{c1} represent the absorbance values of the hydrogel-treated group, the CCK-8 blank group (medium with CCK-8 only), and the untreated control group incubated for 24 hours, respectively.

For fluorescent staining, cells were seeded and incubated according to the established protocol. At the designated time points, the culture medium was removed, and Calcein-AM solution was subsequently added following the manufacturer's instructions. After a 30 minutes incubation at 37 °C, cellular viability was visualized with a laser scanning confocal microscope (TCS SP8, Leica, Germany).

2.6 *In vitro* antimicrobial activity of the HA-B@Fe hydrogel

The antimicrobial efficacy of HA-B_1@Fe, HA-B_2@Fe, and HA-B_3@Fe hydrogels was assessed using a plate coating assay, bacterial growth curve analysis, and SEM. Prior to testing, hydrogels were sterilized under UV for 2 hours. *S. aureus* and *E. coli* were pre-cultured in TSB under shaking conditions at 37 °C and 150 rpm for 8 hours to reach the exponential growth phase.

For the plate coating assay, 1 g of hydrogel was dispersed with 30 mL of normal saline. Subsequently, 1 mL of bacterial suspension (1×10^7 CFU mL^{-1}) was added to the mixture. To ensure thorough contact between the hydrogel and bacteria, the suspension was agitated on an orbital shaker at 37 °C and 150 rpm for 2 hours. Following incubation, 0.1 mL of the resulting mixture was spread onto tryptone soya agar (TSA) plates and incubated at 37 °C for 24 hours. The bacteriostatic rate was calculated using the following formula:

$$\text{Bacteriostatic rate}(\%) = \frac{A - B}{B} \times 100$$

where A and B are the number of bacterial colonies of the blank (control) and test samples, respectively.

Bacterial growth kinetics in the presence of HA-B@Fe hydrogels were analyzed by monitoring the optical density at 600 nm (OD_{600}) every hour over a 14 hours cultivation period under controlled conditions (37 °C, 150 rpm). Growth curves were generated from the time-course OD_{600} data, with all experiments performed in triplicates to ensure reproducibility.

Bacterial morphology was characterized using SEM. Based on the above antibacterial screening results, HA-B_3@Fe hydrogel was selected for morphology observation. *S. aureus* and *E. coli* were co-cultured with the hydrogel in TSB medium for 3 hours. The bacteria were harvested by centrifugation and fixed in 2.5% glutaraldehyde for 48 hours. Untreated bacteria served as the control group. Samples were sequentially dehydrated using ethanol solutions at concentrations of 30%, 50%, 70%, 90%, and 100%, each for 10 min, followed by lyophilization. The dried samples were mounted on aluminum stubs, sputter-coated with gold, and imaged using SEM.

2.7 Evaluation of the healing activity of hydrogels for diabetic wounds

Male ICR mice (18–22 g, 4 weeks-old) were obtained from Beijing Vital River Laboratory Animal Technology Co., Ltd. After a one-week acclimatization period, diabetes was induced by intraperitoneal injections of streptozotocin solution at a dose of 50 mg kg^{-1} for five consecutive days. Blood glucose levels were monitored over the following 2–3 weeks, and mice with blood glucose levels exceeding 16.65 mmol L^{-1} were considered successfully diabetic. The diabetic mice were randomly divided into three groups: control, commercial dressing (business), and HA-B_3@Fe hydrogel treatment. After anesthesia, the dorsal area of each mouse was shaved and depilated to prepare the surgical sites. A full-thickness dorsal wound, with a diameter of 8 mm, was created on the dorsum and covered with the appropriate dressing corresponding to each group. Wound healing process was documented photographing the wound area on days 0, 3, 7, 14, and 21 post-injury. Wound areas were quantified using ImageJ software. Additionally, wound tissues were collected on days 7 and 14, fixed in 4% paraformaldehyde, and subjected to histological processing. Hematoxylin and Eosin (H&E) and Masson trichrome staining were performed to evaluate tissue pathology and collagen deposition, respectively. The stained sections were observed under a light microscope (CX40P, Shunyu, China).

2.8 Statistical analysis

Statistical analyses were performed using GraphPad Prism (GraphPad Software Inc., USA) and Origin Pro (Origin Lab Corporation, USA). All experiments in this study were independently repeated at least three times, and data are presented as mean ± standard deviation (SD). The statistical significance was assessed using a paired Student's *t*-test for two-group comparisons. For comparisons among more than two groups, one-way analysis of variance (ANOVA) was employed. A *P*-value ≤0.05 was considered statistically significant. Significance levels are indicated as follows: $*p < 0.05$, $**p < 0.01$, $***p < 0.001$, and $****p < 0.00001$.

© 2026 The Author(s). Published by the Royal Society of Chemistry

Open Access Article. Published on 03 June 2026. Downloaded on 6/9/2026 5:49:35 AM. This article is licensed under a Creative Commons Attribution-NonCommercial 3.0 Unported Licence.

3 Results and discussion

3.1 Synthesis and characterization of HA-B

To synthesize HA-B, amino-containing polymyxin B was covalently attached to the carboxyl groups of the HA backbone using EDC and HOBt as coupling agents (Fig. 1a). The FTIR spectrum of the HA-B showed significant changes compared to native HA. Notably, an absorption peak corresponding to the amino group ($-NH_2$) appeared at around 3400 cm^{-1}, indicating the conjugation of polymyxin B to the HA polymer chain (Fig. 1b). In the ^1H NMR spectra (Fig. 1c), a distinct chemical shift located at 7.2–7.4 ppm was observed in the HA-B spectrum, attributed to the aromatic protons of the benzene ring present in polymyxin B. This further confirmed the successful grafting of polymyxin B onto HA. The grafting rate was calculated to be approximately 5.76%.

3.2 Fabrication and characterization of the hydrogel

To develop injectable HA-B@Fe hydrogels with shear-thinning behavior and antimicrobial functionality, a pre-formulated Fe^{3+}–EDTA complex was used as a cross-linking agent. The complex facilitates coordination Fe^{3+} ions and the carboxyl groups on HA-B, forming a three-dimensional network through metal–ligand interactions. Briefly, $Fe_2(SO_4)_3$ and EDTA were dissolved in deionized water to formulate a 0.05 mol L^{-1} Fe^{3+}–

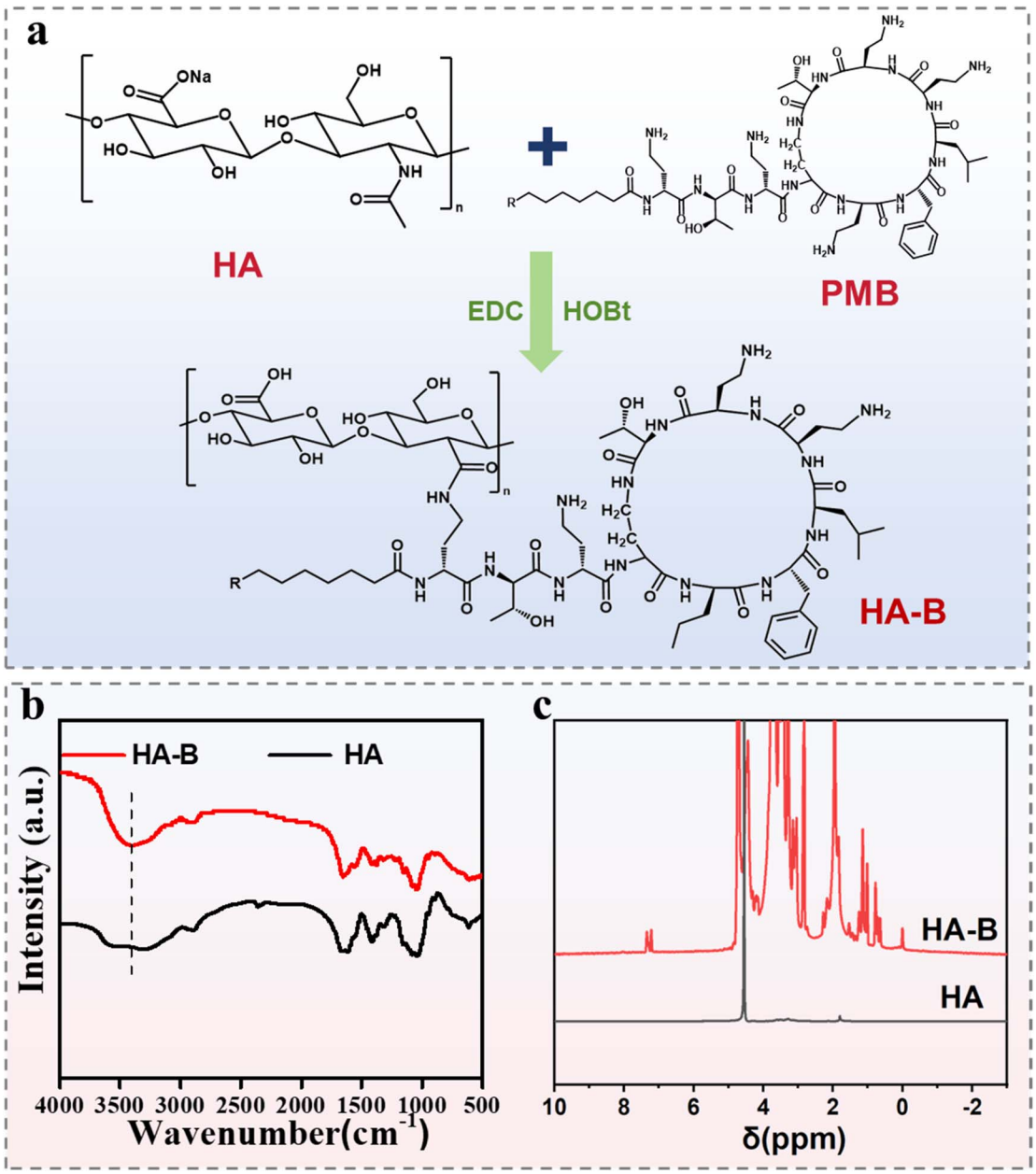

Fig. 1 (a) Schematic illustration of the synthesis of polymyxin B-grafted hyaluronic acid (HA-B); (b) FTIR spectra comparing HA-B and native HA; (c) ^1H NMR spectra of HA-B and HA, confirming successful grafting of polymyxin B onto the HA backbone.

Open Access Article. Published on 03 June 2026. Downloaded on 6/9/2026 5:49:35 AM.
This article is licensed under a Creative Commons Attribution-NonCommercial 3.0 Unported Licence.

EDTA complex solution. This solution was then added to HA-B solutions (prepared at 1%, 2%, and 3% (w/v) concentrations) at a volume ratio of 1 : 5 (Fe^{3+}–EDTA : HA-B), followed by magnetic stirring to promote uniform gelation. As shown in Fig. 2a, gelation did not occur in the absence of Fe^{3+}–EDTA complex, confirming that this coordination complex played a key role in hydrogel preparation.

It is worth noting that the Fe^{3+}–EDTA complex rapidly formed hydrogels upon mixing with different HA-B solutions of various concentrations, with gelation occurring within 10 s under magnetic stirring. This rapid *in situ* gelation is critical for

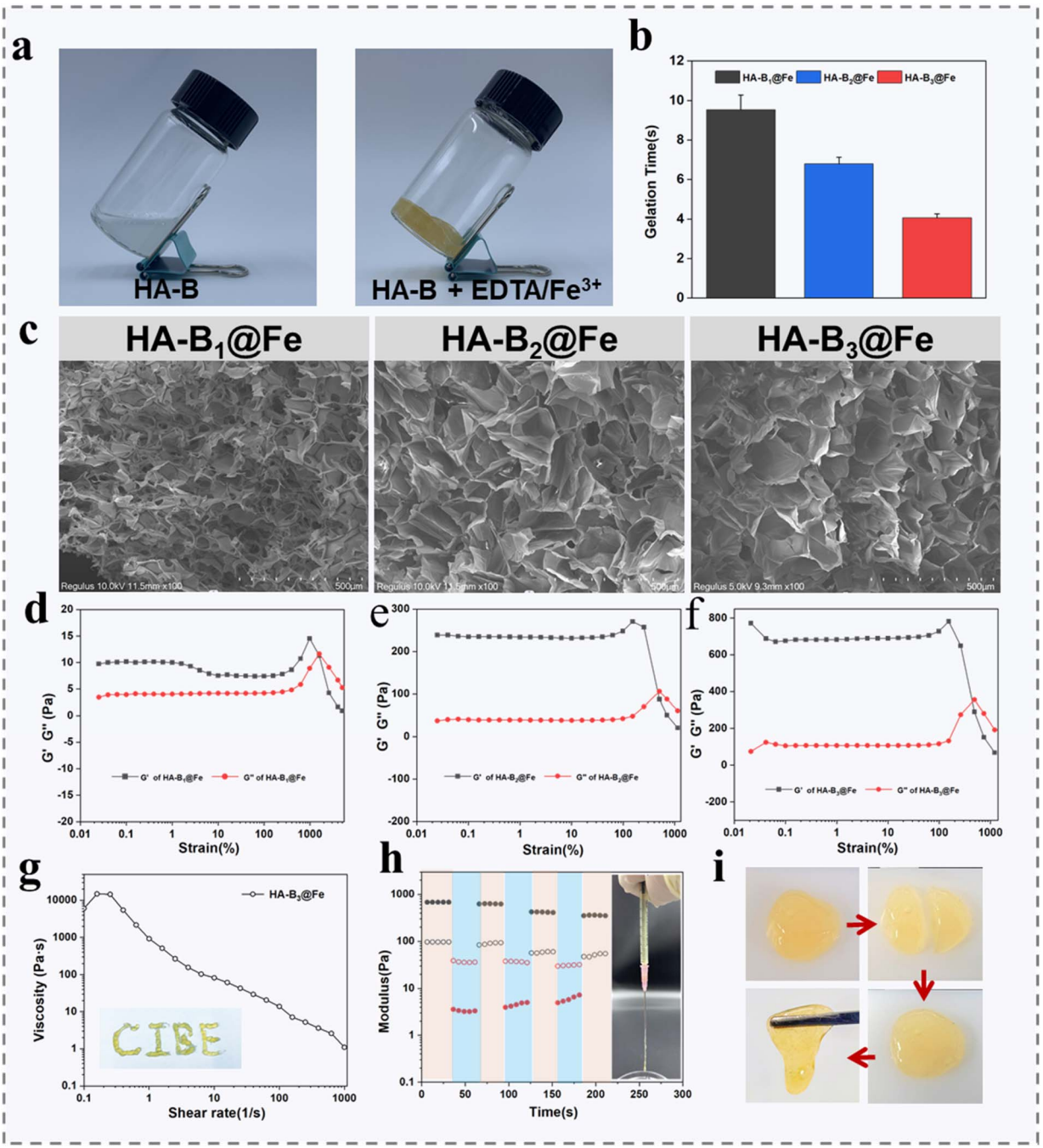

Fig. 2 (a) Photographs of HA-B_3@Fe hydrogel formation; (b) gelation time of HA-B@Fe hydrogel with varying HA-B concentrations; (c) SEM images showing the porous microstructure of HA-B_1@Fe, HA-B_2@Fe and HA-B_3@Fe; (d–f) rheological analysis of storage modulus (G') and loss modulus (G') for HA-B_1@Fe (d), HA-B_2@Fe (e) and HA-B_3@Fe (f) under oscillatory strain amplitude sweep; (g) shear rate-viscosity test for determining the shear-thinning behavior of HA-B_3@Fe hydrogel; (h) self-healing behavior of HA-B_3@Fe hydrogel under strains of 1% and 3000%. Inset: photograph illustrating injectability through a syringe; (i) macroscopic photographs of cut and rejoined HA-B_3@Fe hydrogels, visually confirming self-healing behavior.

© 2026 The Author(s). Published by the Royal Society of Chemistry

Open Access Article. Published on 03 June 2026. Downloaded on 6/9/2026 5:49:35 AM. This article is licensed under a Creative Commons Attribution-NonCommercial 3.0 Unported Licence.

clinical applicability, particularly in wound dressing scenarios. The gelation time was assessed by the vial inversion method, and the results are shown in Fig. 2b. As the HA-B concentration increased, the gelation time decreased, likely due to the increased crosslinking sites, which accelerated gel network formation.

Furthermore, the microstructures of the freeze-dried HA-B@Fe hydrogels were analyzed by SEM. As shown in Fig. 2c, all HA-B@Fe hydrogels exhibited a three-dimensional porous network, which is beneficial for retaining moisture and maintaining a moist wound environment. This is a critical factor for promoting wound healing. Additionally, the extracellular matrix-like structure and interconnected pores facilitate oxygen and nutrient exchange, while also supporting cell adhesion and proliferation.[22–24] Collectively, these findings establish the structural and functional suitability of HA-B@Fe hydrogels for applications in chronic wound treatment.

3.3 Mechanical and self-healing properties of hydrogels

For wound dressing applications, hydrogels must possess sufficient mechanical strength to withstand external stress and protect the wound sites. The storage modulus (G') and loss modulus (G'') are key rheological parameters that evaluate the solid-like and liquid-like behaviors of hydrogels, respectively. Therefore, G' and G'' of HA-B_1@Fe, HA-B_2@Fe and HA-B_3@Fe measured using strain sweep tests. As shown in Fig. 2d–f, all three hydrogels exhibited a linear viscoelastic region within the strain range of 0.1–100%, and in each case, the G' exceeded the G'', indicating dominant elastic, solid-like behavior of the hydrogels.

Furthermore, the measured G' values were approximately 10 pa, 234 Pa and 689Pa for HA-B_1@Fe, HA-B_2@Fe and HA-B_3@Fe, respectively, indicating that the mechanical strength of the hydrogels increased with increasing HA-B concentration. This enhancement can be attributed to the higher density of carboxyl groups provided by increased HA-B content, which led to a greater degree of crosslinking with Fe^{3+}–EDTA complexes. As a result, the hydrogel network became more robust, exhibiting improved mechanical properties and energy dissipation. This not only protects the hydrogel from deformation or rupture under external forces, but also helps maintain a stable three-dimensional structure conducive to cell proliferation and migration.

Diabetic wounds often exhibit irregular shapes and depths. Unlike block hydrogels, injectable hydrogels offer advantages of conforming to such irregular wound geometry. For a hydrogel to be injectable, it must satisfy two key criteria: (1) it should possess temporary fluidity under extrusion, and (2) it must rapidly recover its gel structure post-extrusion through self-healing.[25]

To evaluate the injectability of HA-B@Fe hydrogels, rheological analyses were performed, including shear rate-dependent viscosity measurements and alternating strain tests. As shown in Fig. 2g, the viscosity of the hydrogel decreased rapidly with increasing shear rate, indicating the shear thinning behavior. This property enables it to be smoothly extruded through a syringe, allowing complete coverage of irregular wound surfaces. The self-healing capability of hydrogels was investigated by alternating strain sweeps at 1% and 3000%. As shown in the Fig. 2h, the hydrogel's crosslinked network was interrupted under high strain, but rapidly restored under low strain, indicating excellent self-healing behavior. This characteristic is particularly of great significance for wound dressings subjected to mechanical motion damage. Additionally, the self-healing property of the HA-B_3@Fe hydrogel was visually confirmed by macroscopic observation of the cut and rejoined samples, as presented in Fig. 2i, further supporting its potential for practical application in dynamic wound environments.

3.4 Cell viability assay

Hydrogel intended for skin wound repair should exhibit excellent biocompatibility. The *in vitro* cytocompatibility was assessed by using the CCK-8 assay and fluorescence staining with L929 mouse fibroblast cells. Firstly, Calcein-AM was used to visualize live cells after co-culture with HA-B@Fe hydrogels. As can be seen in Fig. 3a, the L929 cells remained high viability and exhibited intact cellular morphology across all HA-B@Fe hydrogel groups, indicting good biocompatibility with the hydrogel material.

To quantitatively determine the cell viability, L929 were incubated with extracts from HA-B_1@Fe, HA-B_2@Fe and HA-B_3@Fe for 24 h, 48 h and 72 h. As shown in Fig. 3b, the viability of treated cells remained above 90% at all time-points. Notably, all HA-B@Fe groups showed greater cell viability than the untreated control group, meeting the ISO10993:2009 standard for biomaterials.[26] These findings prove that the hydrogels possess excellent cytocompatibility and that increasing HA-B concentration does not nagetively affect cell viability. This biocompatibility is likely attributed to the natural origin of hyaluronic acid, a key component of the extracellular matrix (ECM). When cells are co-cultured with the HA-based hydrogel, the ECM-like environment provided by the porous structure supports cell adhesion, proliferation and migration.

3.5 Antimicrobial activity of the HA-B@Fe hydrogel *in vitro*

Polymyxin B is an antibiotic peptide isolated from bacillus polymyxa, well known for its potent bactericidal activity against a wide range of Gram-negative bacteria. In general, its primary action mechanism involves binding to acidic phospholipids and lipopolysaccharides in the outer bacterial cell membranes, disrupting membrane integrity, causing leakage of intracellular components, and ultimately leading to cell death. However, the clinical application of polymyxin B is significantly limited due to its systemic toxicity, particularly nephrotoxicity, ototoxicity, and neuromuscular blockade. In this article, polymyxin B was covalently grafted onto hyaluronic acid backbone to form HA-B, resulting in a non-leaching hydrogel system. This immobilization strategy effectively mitigates the risk of local toxicity associated with excessive local concentration.

To further broaden the antimicrobial spectrum (due to the limited effect of polymyxin B on Gram-positive bacteria), Fe^{3+}

Open Access Article. Published on 03 June 2026. Downloaded on 6/9/2026 5:49:35 AM.
This article is licensed under a Creative Commons Attribution-NonCommercial 3.0 Unported Licence.

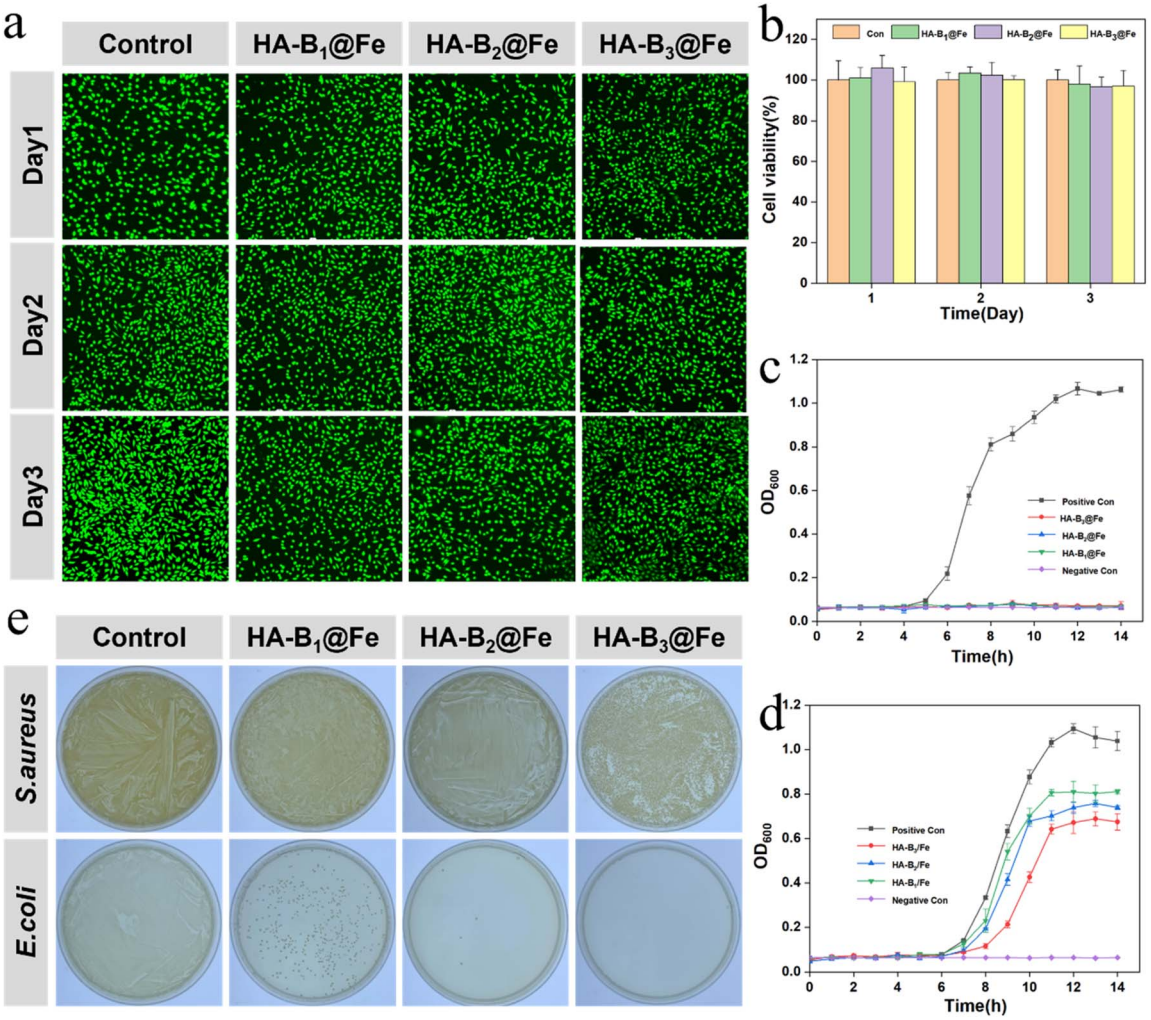

Fig. 3 (a) Live fluorescent images of L929 cells cultured in the hydrogel extract after 24, 48 and 72 h, stained with Calcein-AM to assess cell viability; (b) quantitative analysis of L929 cell proliferation after treatment with hydrogels for 1, 2, and 3 days, as detected by CCK-8 kit; (c) bacterial growth curves in the presence of hydrogels against *E. coli*; (d) bacterial growth curves in the presence of hydrogels against *S. aureus*; (e) representative images of surviving bacterial colonies on TSA plates after exposure to HA-B_1@Fe, HA-B_2@Fe and HA-B_3@Fe.

ions were introduced as cross-linking agents to prepare HA-B@Fe hydrogels. These metal ions not only facilitate hydrogel network formation through coordination with carboxyl groups but also provide inherent antibacterial activity. As a result, the HA-B@Fe hydrogel exhibits synergistic antimicrobial efficacy against both Gram-positive and Gram-negative bacteria. Analysis of bacterial growth kinetics confirmed that treatment with HA-B@Fe hydrogels led to potent inhibition of *E. coli* proliferation, with growth being fully arrested within 14 hours irrespective of the hydrogel concentration tested (Fig. 3c). In contrast, when *S. aureus* was exposed to the hydrogels, the antibacterial effect showed a moderate concentration-dependent trend, with higher concentrations showing more pronounced inhibition (Fig. 3d). To further validate the antimicrobial efficacy of HA-B@Fe hydrogels, agar plate assays and bacterial growth curve analysis were performed. As shown in Fig. 3e, colony formation of *E. coli* was almost completely suppressed across all hydrogel concentrations, with minimal to no viable colonies viable on culture plates, confirming the potent bactericidal activity of the hydrogels against Gram-negative bacteria. For *S. aureus*, although bacterial growth was not completely inhibited in all hydrogel-treated groups, colony counts were substantially reduced compared to the untreated control, indicating a concentration-dependent antibacterial activity primarily mediated by the HA-B component. Notably, since Fe^{3+} concentrations were standardized across experimental groups, the observed inhibitory activity against *S. aureus* is likely attributable to the mild bacteriostatic effect of polymyxin B against this Gram-positive pathogen. The inhibition rates calculated based on the number of colonies are shown in Fig. 4a. The inhibition rates of HA-B_1@Fe, HA-B_2@Fe and HA-B_3@Fe against *S. aureus* were 94.65%, 98.24% and 99.14%, respectively. The antibacterial rate against *E. coli* all exceeded 99.99%.

To further investigate the antibacterial mechanism, SEM was used to observe the morphological changes of the bacteria

© 2026 The Author(s). Published by the Royal Society of Chemistry

Open Access Article. Published on 03 June 2026. Downloaded on 6/9/2026 5:49:35 AM.
This article is licensed under a Creative Commons Attribution-NonCommercial 3.0 Unported Licence.

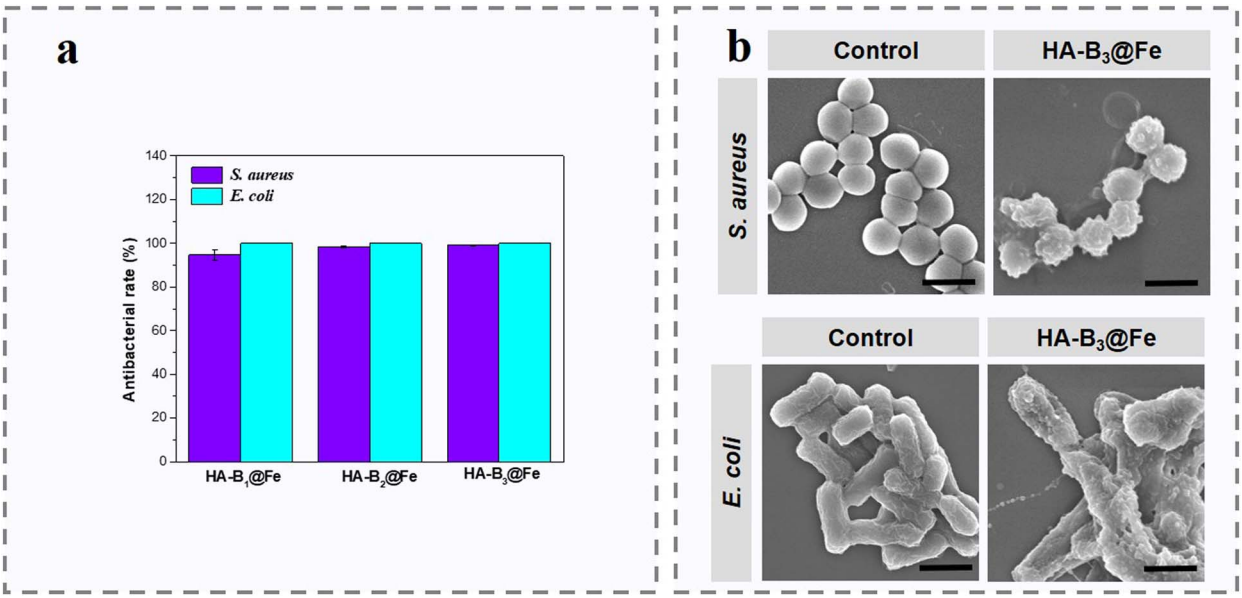

Fig. 4 (a) Inhibition rates of HA-B@Fe hydrogel against *E. coli* and *S. aureus*; (b) SEM images of *S. aureus* and *E. coli* treated with the HA-B_3@Fe hydrogel.

following treatment with HA-B@Fe hydrogel. As shown in Fig. 4b both *E. coli* and *S. aureus* in the control group displayed intact and plump cellular morphology. In contrast, bacteria treated with HA-B@Fe hydrogel exhibited pronounced surface deformation, including wrinkling and surface collapse. These findings clearly demonstrate the strong antibacterial activity of HA-B@Fe hydrogels, with particularly potent effects against Gram-negative *E. coli*, and measurable inhibition against *S. aureus* through combined mechanisms involving both Fe^{3+} coordination and Polymyxin B functionalization.

3.6 Evaluation of the healing activity of hydrogels for diabetic wounds

The therapeutic efficacy of HA-B@Fe hydrogel in promoting diabetic wound healing was evaluated using a standardized full-thickness skin defect model in diabetic mice. Cycle dorsal wounds (8 mm in diameter) were created using a skin biopsy punch after successful induction of diabetes. The mice were randomly divided into three experimental groups: (a) a commercial wound dressing group (commercial), (2) the HA-B@Fe hydrogel treatment group, and (3) a Tegaderm film group served as the untreated control. Wound healing progression was systematically monitored through standardized photographic documentation and clinical evaluation on days 3, 7, 14, and 21 post-injury. The experimental timeline and surgical intervention schedule are illustrated in Fig. 5a. This longitudinal experimental design enabled the comparative evaluation of tissue regeneration and wound contraction under hyperglycemic conditions across different wound management modalities. The wound healing progression, as depicted in Fig. 5b and c, reveals distinct therapeutic differences among the treatment groups over time. Quantitative measurements of wound area are presented in Fig. 5d. Specifically, on day 3, the HA-B_3@Fe hydrogel group showed more significantly wound contraction compared to the other treatment groups, along with the formation of visible membrane-like tissue. In contrast, minor infection was observed in the commercial dressing group. By day 7, the HA-B_3@Fe group showed a significant reduction in wound area size (19%), while the control and commercial dressing groups remained larger wound sizes of approximately 36% and 32%, respectively. By day 21, wounds treated with HA-B_3@Fe hydrogel were nearly fully healed, accompanying by substantial hair regrowth. In comparison, the control group still exhibited visible trauma and incomplete re-epithelialization, confirming the superior wound healing efficacy of the HA-B_3@Fe hydrogel. The accelerated healing observed in the HA-B_3@Fe group is attributed to the ability of the hydrogel to maintain a moist wound environment, promote tissue regeneration, and manage exudate. The porous three-dimensional structure facilitates nutrient and gas exchange while facilitating cell migration and proliferation.

3.7 Evaluation of skin regeneration effects

Epithelial tissue regeneration is important for effective diabetic wound healing and was assessed using Masson's staining and HE staining. As shown in the Fig. 6a, by day 3, no group exhibited fully formed epidermis or granulation tissue. By day 7, all groups exhibited a strong inflammatory response, with the infiltration of inflammatory cells, which is an essential prerequisite for initiating fibroblast migration and wound healing. Interestingly, the HA-B@Fe hydrogel group showed a significant transition from inflammation into proliferative phase, as evidenced by increased fibroblast activity and the presence of dense connective tissue. Granulation tissue integrity is a pivotal role in wound healing, as it fills the wound bed and serves as a scaffold for angiogenesis and re-

Open Access Article. Published on 03 June 2026. Downloaded on 6/9/2026 5:49:35 AM.
This article is licensed under a Creative Commons Attribution-NonCommercial 3.0 Unported Licence.

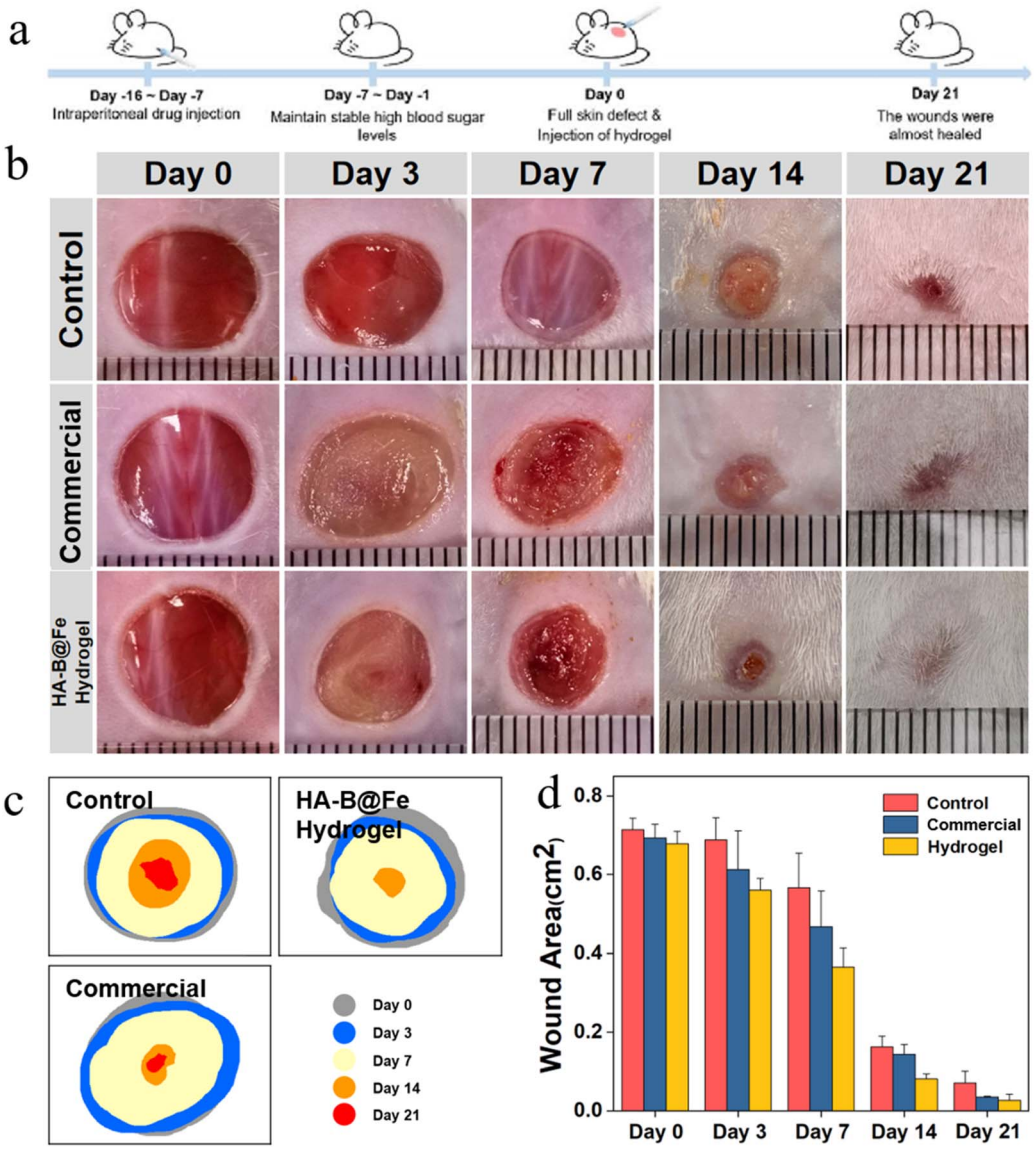

Fig. 5 HA-B_3@Fe hydrogel accelerates diabetic wound healing. (a) Schematic illustration of the diabetic full-thickness skin wound model and the treatment protocol with hydrogel; (b) representative photographs of wound sites on days 0, 3, 7, 14, and 21 post-treatment across different groups; (c) overlapping outlines of the wound closure at each time point to visually compare healing progression among groups; (d) quantitative analysis of wound area at different times ($n = 3$ per group), showing accelerated wound contraction in the HA-B_3@Fe group.

epithelialization. By day 14, wound tissues treated with HA-B@Fe hydrogel exhibited increased fibroblast migration, decreased inflammatory cell infiltration, and the formation of both new epidermal and granulation tissues, which signifies the completion of re-epithelialization and dermal tissue regeneration. In contrast, the control and commercial groups continued to show significant inflammatory cell presence, indicating delayed progression through the wound healing phases.

At day 21, the HA-B@Fe hydrogel group treated wounds demonstrated a thickened and structurally restored epidermis, and complete re-epithelialization. Inflammation was further diminished, and the dermis was morphologically complete and well-organized. In contrast, the control and commercial dressing groups also achieved complete epithelial coverage, but they failed to fully restore the skin structure architecture, with signs of structural collapse still evident.

As shown in Fig. 6b, Masson staining revealed early collagen alignment in the HA-B@Fe hydrogel group. By day 7 and day 21, dense, structurally aligned collagen fibers had formed, indicating advanced ECM remodeling and much faster collagen deposition compared to the other two groups. In addition, histological sections revealed the regeneration of hair follicles and sebaceous glands exclusively in the HA-B@Fe-treated group, demonstrating its superior capacity for dermal regeneration (Fig. 6b). In conclusion, the HA-B@Fe hydrogel facilitated the regeneration of a relatively intact epidermis and dermis, characterized by a highly ordered fibro-collagen structure, closely resembling the histopathological structure of healthy

© 2026 The Author(s). Published by the Royal Society of Chemistry

Open Access Article. Published on 03 June 2026. Downloaded on 6/9/2026 5:49:35 AM.
This article is licensed under a Creative Commons Attribution-NonCommercial 3.0 Unported Licence.

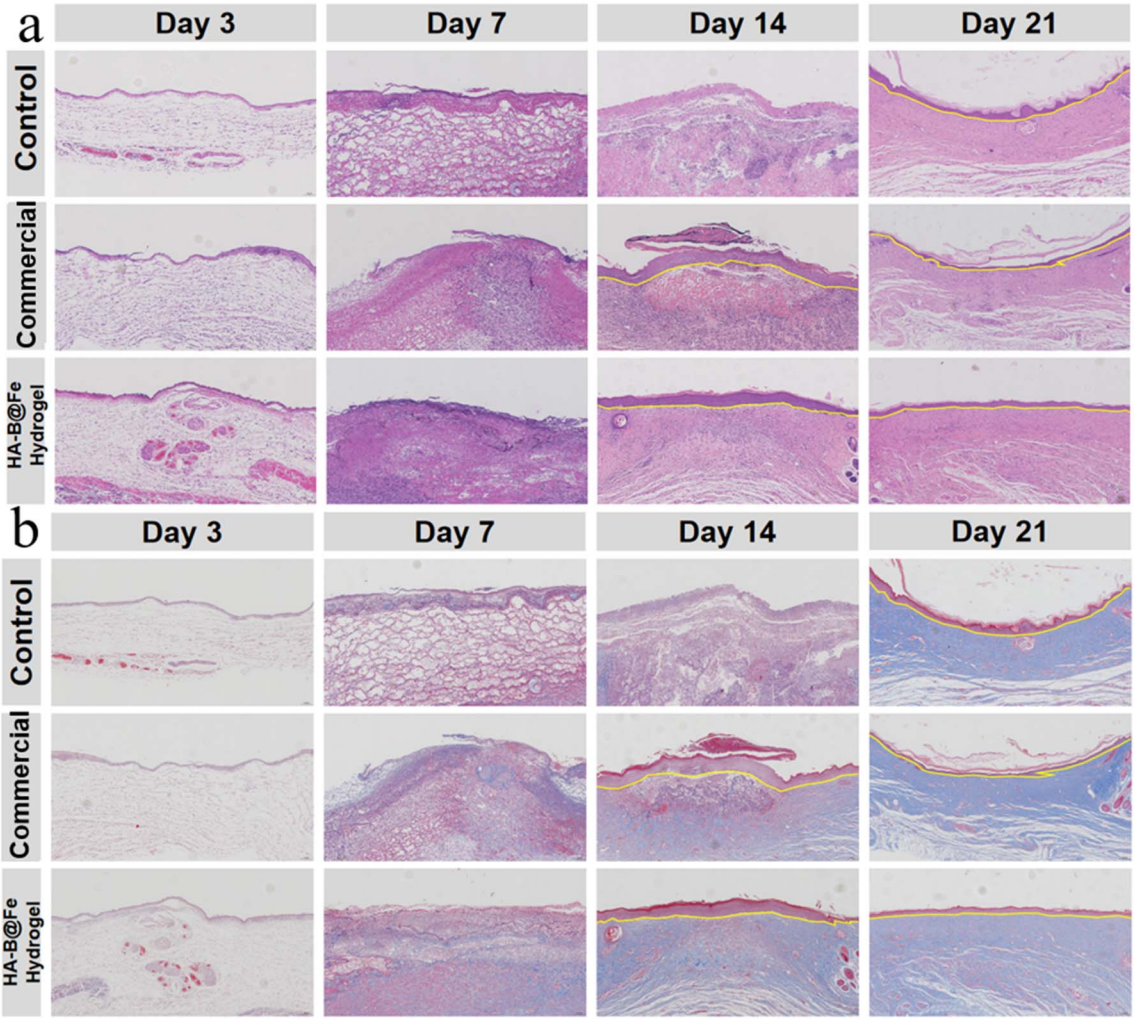

Fig. 6 Histological, immunofluorescence and immunohistochemical analysis of wound healing across treatment groups. (a) H&E staining of wound tissues on days 3, 7, 14, and 21 post-treatment, illustrating re-epithelialization, inflammatory cell infiltration, granulation tissue formation, and dermal regeneration in the control, commercial dressing, and HA-B@Fe hydrogel groups; (b) Masson staining of corresponding wound tissues, showing collagen deposition and organization over time. The HA-B@Fe hydrogel group exhibited denser, more structurally aligned collagen fibers and enhanced dermal remodeling compared to the other groups.

skin tissue. These results demonstrate that the HA-B@Fe hydrogel can effectively reduce inflammation, and accelerate tissue regeneration, and hold significant promise as a therapeutic option for diabetic wound healing.

4 Conclusions

In this study, we developed an HA-B@Fe hydrogel as a promising wound dressing for the effective treatment of diabetic wounds. Polymyxin B was grafted onto hyaluronic acid, harnessing its potent antibacterial activity while mitigating the systemic toxicity commonly associated with its burst release. The resulting HA-B@Fe hydrogel was crosslinked with Fe^{3+}–EDTA through dynamic ionic interactions. The reversible and dynamic metal–ligand interactions endow the HA-B@Fe hydrogel with rapid gelation, shear-thinning injectability, and excellent self-healing capability—properties that are essential for clinical scenarios involving irregular wound coverage and *in situ* application. Furthermore, the hydrogels demonstrated stable mechanical properties, providing strong resistance to external disturbances during use. *In vitro* and *in vivo* assessment confirmed that the HA-B@Fe hydrogels exhibit good biocompatibility and broad-spectrum antimicrobial activity, effectively inhibiting both *E. coli* and *S. aureus*. In a diabetic mouse wound model, HA-B@Fe treatment significantly accelerated wound closure, enhanced epidermal regeneration, promoted collagen fiber tissue deposition and dermal regeneration. These findings underscore the potential of the HA-B@Fe hydrogel as a multifunctional and clinically viable dressing for the clinical treatment of diabetic wounds.

Author contributions

Conceptualization, M. Z. and W. Z.; methodology, Y. Z.; R. S. and Y. S., software, Y. Z.; validation, M. Z., L. J. and J. Z.; formal analysis, M. Z.; investigation, W. Z.; resources, M. Z. and W. Z.;

Open Access Article. Published on 03 June 2026. Downloaded on 6/9/2026 5:49:35 AM. This article is licensed under a Creative Commons Attribution-NonCommercial 3.0 Unported Licence.

data curation, M. Z. and W. Z.; writing – original draft preparation, M. Z. and W. Z.; writing – review and editing, L. J. and J. Z.; visualization, W. Z.; supervision, L. J. and J. Z.; project administration, L. J.; funding acquisition, L. J. All authors have read and agreed to the published version of the manuscript.

Conflicts of interest

There are no conflicts to declare.

Data availability

The data supporting this article have been included as part of the supplementary information (SI). Supplementary information: additional supplementary figures referenced in the main text. See DOI: https://doi.org/10.1039/d6ra03137d.

Acknowledgements

L. J. acknowledges the funds provided by the Ningbo Natural Science Foundation (2023J370). The authors are also thankful for the financial provided by NIMTE, CAS. M. Z. acknowledges the funds provided by National Natural Science Foundation of China (72274189) and Ningbo Leading Medical&Health Discipline (2026-A23).

References

1 X. Yang, W. Li, Y. Liu, N. Cao, Y. He, Q. Sun and S. Zhou, Charged Fibrous Dressing to Promote Diabetic Chronic Wound Healing, *Adv. Healthcare Mater.*, 2024, **13**, 2302183.
2 Y. Kang, L. Xu, J. Dong, X. Yuan, J. Ye, Y. Fan, B. Liu, J. Xie and X. Ji, Programmed microalgae-gel promotes chronic wound healing in diabetes, *Nat. Commun.*, 2024, **15**, 1042.
3 J. Liu, M. Wu, J. Lu, Q. He and J. Zhang, Janus Intelligent Antibacterial Hydrogel Dressings for Chronic Wound Healing in Diabetes, *ACS Appl. Polym. Mater.*, 2023, **5**, 2596–2606.
4 X. Yang, S. He, J. Wang, Y. Liu, W. Ma, C.-Y. Yu and H. Wei, Hyaluronic acid-based injectable nanocomposite hydrogels with photo-thermal antibacterial properties for infected chronic diabetic wound healing, *Int. J. Biol. Macromol.*, 2023, **242**, 124872.
5 C. Chai, P. Zhang, L. Ma, Q. Fan, Z. Liu, X. Cheng, Y. Zhao, W. Li and J. Hao, Regenerative antibacterial hydrogels from medicinal molecule for diabetic wound repair, *Bioact. Mater.*, 2023, **25**, 541–554.
6 S. H. Jeong, S. Cheong, T. Y. Kim, H. Choi and S. K. Hahn, Supramolecular Hydrogels for Precisely Controlled Antimicrobial Peptide Delivery for Diabetic Wound Healing, *ACS Appl. Mater. Interfaces*, 2023, **15**, 16471–16481.
7 D. N. Gilbert, R. J. Guidos, H. W. Boucher, G. H. Talbot, B. Spellberg, J. E. Edwards Jr, W. Michael Scheld, J. S. Bradley and J. G. Bartlett, The 10 × '20 Initiative: Pursuing a Global Commitment to Develop 10 New Antibacterial Drugs by 2020, *Clin. Infect. Dis.*, 2010, **50**, 1081–1083.
8 Z. Saleem, M. A. Hassali and F. K. Hashmi, Pakistan's national action plan for antimicrobial resistance: translating ideas into reality, *Lancet Infect. Dis.*, 2018, **18**, 1066–1067.
9 J.-M. Sabatier, Antibacterial Peptides, *Antibiotics*, 2020, **9**, 142.
10 X. Li, S. Zuo, B. Wang, K. Zhang and Y. Wang, Antimicrobial Mechanisms and Clinical Application Prospects of Antimicrobial Peptides, *Molecules*, 2022, **27**, 2675.
11 H. Wang, F. Gao, M. Rafiq, B. Yu, Q. Niu and H. Cong, Screening of an antimicrobial peptide-TWPAL and its application in hydrogels for wound healing, *Mater. Chem. B.*, 2025, **13**, 2418–2430.
12 E. Zattarin, Z. Sotra, E. Wiman, Y. Bas, J. Rakar, L. Berglund, A. Starkenberg, E. M. Björk, H. Khalaf, K. Oksman, T. Bengtsson, J. P. E. Junker and D. Aili, Controlled release of antimicrobial peptides from nanocellulose wound dressings for treatment of wound infections, *Mater. Today Bio*, 2025, **32**, 101756.
13 Y. Li, D. Hao, G. Feng and F.-J. Xu, A hydrogel wound dressing ideally designed for chronic wound care, *Matter*, 2023, **6**, 1060–1062.
14 Y. Liang, J. He and B. Guo, Functional Hydrogels as Wound Dressing to Enhance Wound Healing, *ACS Nano*, 2021, **15**, 12687–12722.
15 D. Yang, W. Zhao, S. Zhang, Y. Liu, J. Teng, Y. Ma, R. Huang, H. Wei, H. Chen, J. Zhang and J. Chen, Dual Self-Assembly of Puerarin and Silk Fibroin into Supramolecular Nanofibrillar Hydrogel for Infected Wound Treatment, *Adv. Healthcare Mater.*, 2024, **13**, 2400071.
16 X. Lin, X. Yang, P. Li, Z. Xu, L. Zhao, C. Mu, D. Li and L. Ge, Antibacterial Conductive Collagen-Based Hydrogels for Accelerated Full-Thickness Wound Healing, *ACS Appl. Mater. Interfaces*, 2023, **15**, 22817–22829.
17 B. Huang, D. Hu, A. Dong, J. Tian and W. Zhang, Highly Antibacterial and Adhesive Hyaluronic Acid Hydrogel for Wound Repair, *Biomacromolecules*, 2022, **23**, 4766–4777.
18 E. A. Kamoun, E.-R. S. Kenawy and X. Chen, A review on polymeric hydrogel membranes for wound dressing applications: PVA-based hydrogel dressings, *J. Adv. Res.*, 2017, **8**, 217–233.
19 M. Contardi, D. Kossyvaki, P. Picone, M. Summa, X. Guo, J. A. Heredia-Guerrero, D. Giacomazza, R. Carzino, L. Goldoni, G. Scoponi, F. Rancan, R. Bertorelli, M. Di Carlo, A. Athanassiou and I. S. Bayer, Electrospun polyvinylpyrrolidone (PVP) hydrogels containing hydroxycinnamic acid derivatives as potential wound dressings, *Chem. Eng. J.*, 2021, **409**, 128144.
20 H. Alkhoury, A. Hautmann, B. Fuhrmann, F. Syrowatka, F. Erdmann, G. Zhou, S. Stojanović, S. Najman and T. Groth, Studies on the Mechanisms of Anti-Inflammatory Activity of Heparin- and Hyaluronan-Containing Multilayer Coatings—Targeting NF-κB Signalling Pathway, *Int. J. Mol. Sci.*, 2020, **21**, 3724.
21 L. Long, C. Hu, W. Liu, C. Wu, L. Lu, L. Yang and Y. Wang, Injectable multifunctional hyaluronic acid/methylcellulose

© 2026 The Author(s). Published by the Royal Society of Chemistry

Open Access Article. Published on 03 June 2026. Downloaded on 6/9/2026 5:49:35 AM.
This article is licensed under a Creative Commons Attribution-NonCommercial 3.0 Unported Licence.

hydrogels for chronic wounds repairing, *Carbohydr. Polym.*, 2022, **289**, 119456.
22 R. Liu, J. Cai, N. Qin, K. Zhang, T. Li, H. Luo and D. Guo, Nontoxic chemical crosslinked bacterial cellulose-heparin-gelatin composite hydrogel as antibacterial dressing, *J. Mater. Sci. Technol.*, 2024, **178**, 29–38.
23 A. Nurzynska, K. Klimek, I. Swierzycka, K. Palka and G. Ginalska, Porous Curdlan-Based Hydrogels Modified with Copper Ions as Potential Dressings for Prevention and Management of Bacterial Wound Infection—An *In Vitro* Assessment, *Polymers*, 2020, **12**, 1893.
24 S. Tavakoli and A. S. Klar, Advanced Hydrogels as Wound Dressings, *Biomolecules*, 2020, **10**, 1169.
25 P. Bertsch, M. Diba, D. J. Mooney and S. C. G. Leeuwenburgh, Self-Healing Injectable Hydrogels for Tissue Regeneration, *Chem. Rev.*, 2023, **123**, 834–873.
26 ISO 10993: 2018, *Biological Evaluation of Medical Devices*, International Organization for Standardization: Geneva, Switzerland, 2018.